

Spin-glass behavior of $A\text{Fe}_4\text{Al}_8$ ($A = \text{Th}, \text{U}, \text{Np}$) intermetallics

J. Gal

Nuclear Engineering Department, Ben-Gurion-University of the Negev, 84105 Beer Sheva, Israel;
Nuclear Research Center, 84190 Beer-Sheva, Israel;
and Physik Department E15, Technische Universität München, D-8046 Garching bei München, West Germany

I. Yaar, D. Regev, S. Fredo, G. Shani, and E. Arbaboff

Nuclear Engineering Department, Ben-Gurion-University of the Negev, 84105 Beer Sheva, Israel
and Nuclear Research Center, 84190 Beer-Sheva, Israel

W. Potzel, K. Aggarwal, J. A. Pereda, and G. M. Kalvius

Physik Department E15, Technische Universität München, D-8046 Garching bei München, West Germany

F. J. Litterst

Institut für Metallphysik, Technische Universität Braunschweig, D-3000 Braunschweig, West Germany
and Physik Department E15, Technische Universität München, D-8046 Garching bei München, West Germany

W. Schäfer and G. Will

Mineralogisches Institut der Universität Bonn, D-5300 Bonn, West Germany and Kernforschungsanlage, D-5170 Jülich, West Germany

(Received 12 March 1990; revised manuscript received 22 May 1990)

Combined ac- and dc-susceptibility, neutron-diffraction, and Mössbauer studies of UFe_4Al_8 , NpFe_4Al_8 , and ThFe_4Al_8 argue for the establishment of a spin-glass (SG) state below $T_{\text{SG}}(B \rightarrow 0) \approx 130, 120$, and 110 K, respectively. The SG temperature $T_{\text{SG}}(B)$ decreases with application of external magnetic field B . The ac susceptibility (χ_{ac}) shows a sharp cusp at $T_{\text{SG}}(B \approx 0)$. The isothermal and thermoremanent magnetization differ markedly and show temperature-dependent irreversibilities below $T_{\text{SG}}(B)$. The Mössbauer spectra reveal onset of hyperfine splitting, indicating frozen spins below $T_{\text{SG}}(0)$. The neutron-diffraction studies of UFe_4Al_8 and NpFe_4Al_8 show that after switching off the external magnetic field greater than 3 T the U and Np momenta ($2a$ site) are frozen parallel to the direction of the external field. We label the freezing temperature under high external fields T_{OG} , and show that it serves as the upper limit of $T_{\text{SG}}(B)$ with $T_{\text{SG}}(B \rightarrow 0) \rightarrow T_{\text{OG}}$. For concentrated SG systems, $T_{\text{SG}}(0)$ is a reproducible value, independent of the observation time window, which indicates a true thermodynamic phase transition; the cusp in χ_{ac} , however, is not necessarily a confirmation for the establishment of a SG state.

I. INTRODUCTION

The nature of the magnetic transition associated with the spin-glass (SG) state and its correlation with the cusp observed in the ac susceptibility is still controversial. It is not clear whether the transition observed is a true thermodynamic phase transition or whether it represents some type of nonequilibrium effect that depends on the experimental time window through which one is observing phenomena with anomalously long relaxation times.¹⁻³ In addition, little is known about the magnetic properties of the concentrated SG systems. Some Monte Carlo simulations of dilute SG systems predict that the ac susceptibility should exhibit smooth, round, maximum behavior and no cusp.¹ This fact was taken as evidence that no transition occurs.⁴ It was later pointed out by Stauffer and Binder¹ that the Monte Carlo calculations are equally consistent with a phase transition and that no firm statement can be made even if the calculations reveal no cusp.

Traditionally, designation of a system as a spin glass is

based in the first instance on experimental observation of a cusp in the ac susceptibility and also on nonlinear terms in the field dependence of the magnetization below the SG transition temperature T_{SG} . In addition, this assignment should be confirmed by other properties, like irreversibilities (history effects) in the dc magnetization and frozen local spin ordering.⁵ All these effects should be associated with lack of a long-range magnetic order below T_{SG} , as confirmed by neutron Bragg scattering.² We have recently reported on the $R\text{Fe}_4\text{Al}_8$ ($R = \text{Ho}, \text{Er}, \text{Dy}$) system which displays a spin-glass behavior; however, no cusp in the ac susceptibility in the vicinity of T_{SG} was observed.⁵ In the present contribution we show that magnetic frustration leads to a spin-glass state also in the isostructural actinide counterparts, the $A\text{Fe}_4\text{Al}_8$ ($A = \text{Th}, \text{U}, \text{Np}$) intermetallics. Contrary to the $R\text{Fe}_4\text{Al}_8$ compounds, their SG transitions are characterized by a sharp cusp in the ac susceptibility at T_{SG} . In addition, $T_{\text{SG}}(B)$ decreases with application of external magnetic fields. We attribute these differences to $5f$ -electron itinerant behavior which influences the character of the

interactions in a spin-glass system.

Our Mössbauer, ac- and dc-susceptibility results furnish evidence that T_{SG} represents a true thermodynamical phase transition in the systems investigated. In addition, we argue that for concentrated SG systems, the SG transition is not necessarily associated with a cusp in χ_{ac} , in accord with the theoretical calculations for dilute SG systems.

II. EXPERIMENTAL

The AFe_4Al_8 ($A=Th,U,Np$) intermetallics were prepared by arc melting of nominal amounts of the constituents in a dry argon atmosphere. An x-ray $Cu K\alpha_1$ Guinier transmission pattern of the powder showed that the specimens were of a single phase, consistent with the $I4/mmm$ space group.⁶ This was further confirmed by the nuclear reflections of our neutron-diffraction measurements, performed on the powder diffractometer KATINKA of Bonn University at the KFA-Jülich. This diffractometer is equipped with the linear position-sensitive detector JULIOS.⁷ The wavelength used was 1.09 Å.

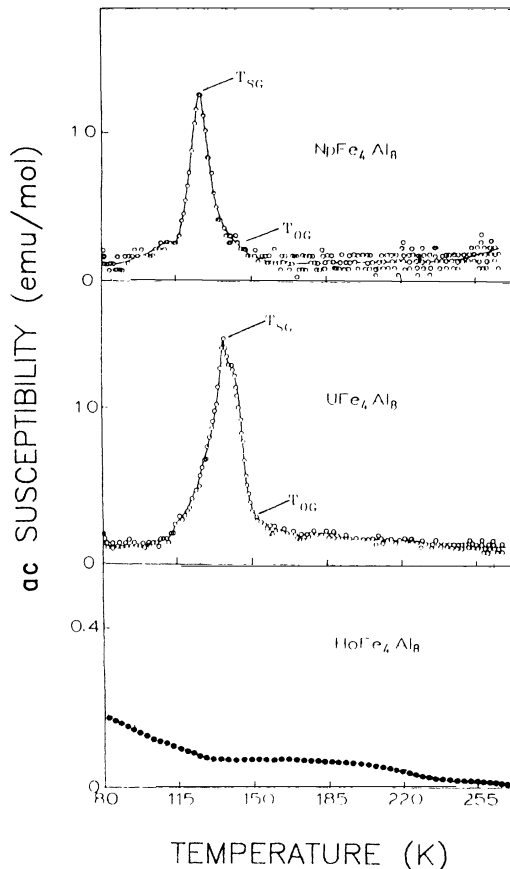


FIG. 1. ac-susceptibility curves as a function of temperature for $NpFe_4Al_8$ and UFe_4Al_8 above 80 K. No cusp is observed in $HoFe_4Al_8$ as shown for comparison. The open circles represent measurements taken with the low-sensitivity susceptometer, and the dots represent the high-sensitivity susceptometer ($\approx 10^{-7}$ emu/g); see text.

The ^{57}Fe 14-keV and ^{237}Np 60-keV Mössbauer transmission experiments were carried out in a conventional, variable-temperature cryostat. The dc magnetization measurements were performed with a vibrating sample magnetometer described elsewhere.^{8,9} Two types of ac susceptometers were used for the detection of T_{SG} : a triple-coil ac susceptometer⁸ and a high-sensitivity ac susceptometer ($\approx 10^{-7}$ emu/g). The magnetic field at the sample was ≈ 8 G.

III. EXPERIMENTAL RESULTS

A. UFe_4Al_8 and $NpFe_4Al_8$

The ac susceptibilities of UFe_4Al_8 and $NpFe_4Al_8$ are displayed in Fig. 1. The curves show an upturn at 150(5) and 130(5) K with sharp maxima at $T_{SG} \approx 130(5)$ and

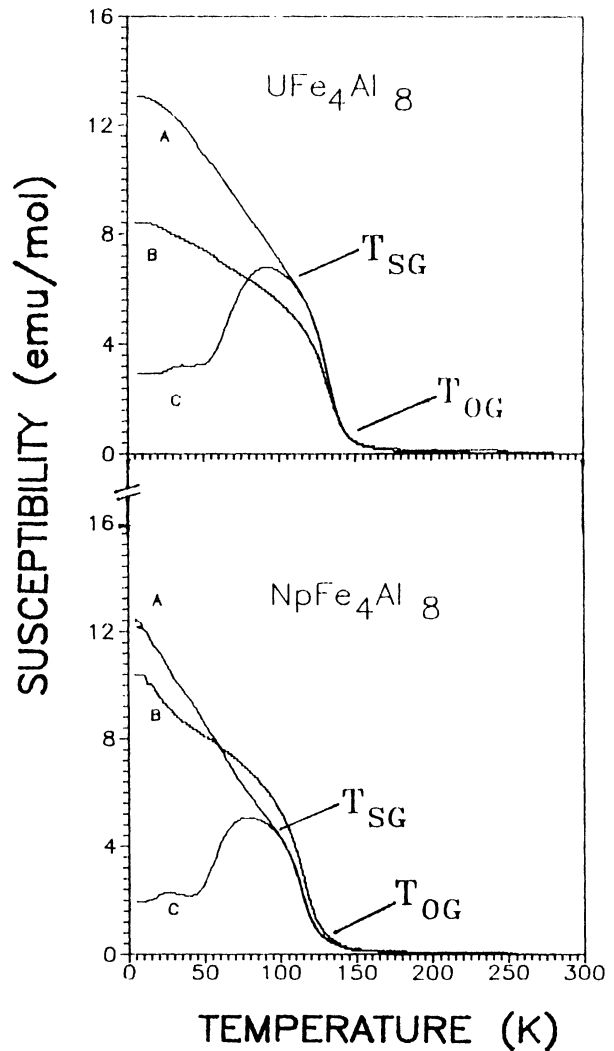


FIG. 2. dc magnetization in $NpFe_4Al_8$ and UFe_4Al_8 . A, cooled under applied external magnetic field (FC) of 2 T and measured under 0.1 T. B, cooled in 0.03 T. A magnetic field of 2 T was switched on for only 5 min. The measurements were performed in an applied field of 0.1 T. C, cooled under 0.03 T and measured under 0.1 T.

120(5) K, respectively. Such a behavior can be attributed either to a ferromagnetic or to a SG transition at T_{SG} .²

The dc magnetization measurements of UFe_4Al_8 and NpFe_4Al_8 were performed under applied magnetic fields from 0.03 to 0.5 T. Some of the isothermal and thermoremanent magnetization curves are displayed in Figs. 2 and 3. Upturns of the magnetization curves, under the applied fields, indicating magnetic phase transitions, are clearly recognized at about 145 and 130 K for UFe_4Al_8 and NpFe_4Al_8 , respectively. We label these upturns T_{OG} and will show below that they represent the upturns ob-

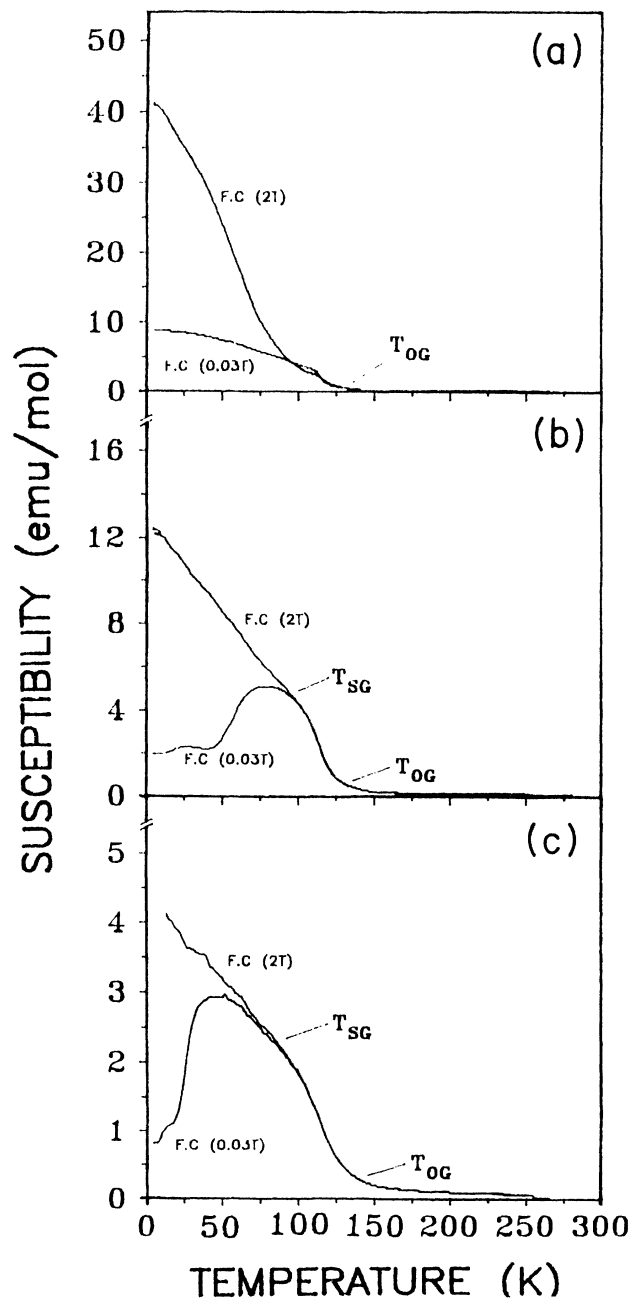


FIG. 3. Thermoremanent dc magnetization of NpFe_4Al_8 performed at various applied magnetic fields: (a) 0.03 T, (b) 0.1 T, (c) 0.3 T. T_{SG} is dependent on the applied magnetic field.

served by the ac susceptibility (Fig. 1), and coincide with the freezing temperatures of the actinide (A) moments ($2a$ site) aligned in a strong magnetic field as determined by our neutron-diffraction experiments.

The samples were cooled under applied fields (FC) of 0.03 and 2 T. The appearance of thermoremanent effects, as demonstrated in Figs. 2 and 3, is typical of spin-glass behavior. The spin-glass transition temperature T_{SG} is defined as the temperature at which the thermoremanent component of the magnetization vanishes, namely, where the two curves shown in Fig. 3 coincide. T_{SG} is strongly dependent on the applied magnetic field B under which the experiment is performed and is assigned as $T_{\text{SG}}(B)$. As shown in Fig. 3(a), $T_{\text{SG}}(B \rightarrow 0) \rightarrow T_{\text{OG}}$. A nonlinear behavior of $T_{\text{SG}}(B)$ is clearly demonstrated in Fig. 4. By extrapolation to zero applied field, we derive $T_{\text{SG}}(0)$ as 138 ± 5 and 118 ± 5 K for UFe_4Al_8 and NpFe_4Al_8 , respectively.

The ^{57}Fe Mössbauer studies of UFe_4Al_8 and NpFe_4Al_8 show the onset of magnetic hyperfine splitting below ≈ 140 and ≈ 125 K, respectively. We label these temperatures $T_{\text{SG}}(0)$, in good agreement with our ac- and dc-susceptibility measurements. Typical spectra are displayed in Figs. 5(a) and 5(b). The spectra of UFe_4Al_8 and NpFe_4Al_8 , and their temperature dependencies, are quite similar. They are composed basically of the spectra of two nonequivalent sites representing Fe in the $8f$ ($\approx 96\%$) and Fe in the Al atomic positions $8j$ ($\approx 4\%$).¹⁰ The ^{57}Fe spectra show nonmagnetic quadrupole splitting from room temperature down to the respective $T_{\text{SG}}(0)$ (Fig. 5). Below $T_{\text{SG}}(0)$ a superposition of paramagnetic and magnetically split patterns develops. The spectra could be satisfactorily fitted by assuming a distribution of magnetic hyperfine fields. The hyperfine parameters for the Fe ($8f$ site) are summarized in Table I. The relative fraction of the paramagnetic and magnetically ordered Fe, as derived from the relative absorption intensities of the magnetic and paramagnetic patterns, is given for both samples in Fig. 6. Note the differences in the effective quadrupole interaction between the magnetic (q_M) and

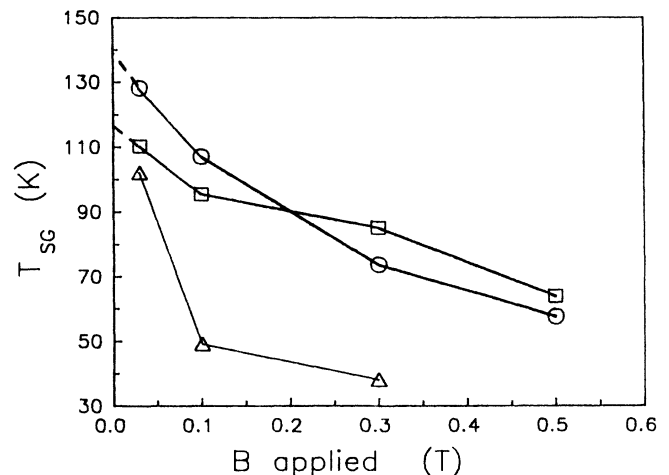


FIG. 4. Magnetic field dependence of the spin-glass temperature T_{SG} , for UFe_4Al_8 (\circ), NpFe_4Al_8 (\square), and ThFe_4Al_8 (\triangle).

the paramagnetic (q_P) states of ^{57}Fe in the $8f$ sites, indicating an angle of $\approx 90^\circ$ between the magnetic direction and the electric field gradient (Table I).

The ^{237}Np Mössbauer spectra of NpFe_4Al_8 show a magnetically split pattern, indicating local spin ordering below 120 K. The Mössbauer spectra at 4.2 and 130 K are depicted in Fig. 7. The distribution of hyperfine fields at the Np nucleus below 120 K and down to 4 K is more strongly pronounced compared to the Fe case. This is related to the higher sensitivity of the ^{237}Np nucleus to

small changes in the hyperfine fields due to random distributions of Al vacancies, or Fe in Al positions.^{5,10}

The neutron-diffraction patterns of NpFe_4Al_8 and UFe_4Al_8 show enhancement of several reflections on approaching low temperatures. In UFe_4Al_8 a gradual (non-Brillouin-like) enhancement of the (110) reflection from 150 K down to 4 K is clearly recognizable (Figs. 8 and 9). The (110) reflection shows irreversibilities upon cooling and heating as demonstrated in Figs. 9 and 10. In addition, some weak enhancement of the (310), (112), and (330) reflections is observed, while the (200,101) and (220,211) reflections show irregularities in the integrated

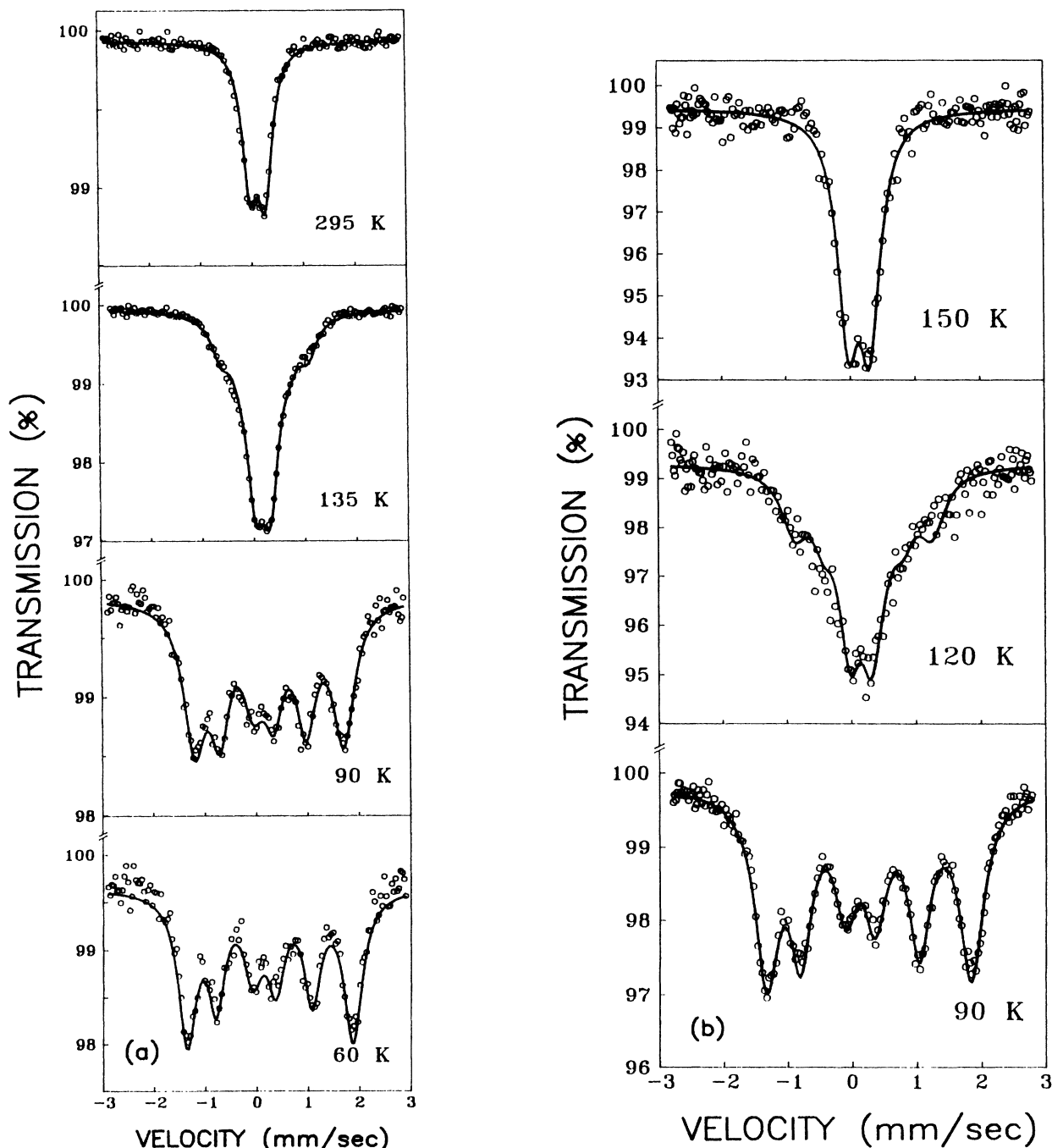


FIG. 5. ^{57}Fe Mössbauer absorption spectra of (a) UFe_4Al_8 and (b) NpFe_4Al_8 , at various temperatures. The solid line represents a least-squares fit assuming superposition of paramagnetic and magnetic states described in the text.

TABLE I. Magnetic and hyperfine properties of $A\text{Fe}_4\text{Al}_8$ and HoFe_4Al_8 . The SG temperatures $T_{\text{SG}}(0)$ are average values derived from ac and dc susceptibilities and Mössbauer data. The freezing temperature of the $2a$ site, T_{OG} , is defined in the text.

Compound		UFe_4Al_8	NpFe_4Al_8	ThFe_4Al_8	HoFe_4Al_8
hyperfine field B_{hf} (T)	^{57}Fe	10.8(5)	9.5(5)	11.4(5)	10.9(5)
	^{237}Np		150 ^a		
effective quadrupole interaction (^{57}Fe) $\frac{1}{2}eqQ(3\cos^2\theta - 1)$ (mm/sec)	$> T_{\text{SG}}$	0.58	0.66	0.23	0.67
	$< T_{\text{SG}}$	+0.26	+0.26	+0.14	+0.25
ratio q_P/q_M		2.44	2.51	3.28	2.68
spin-glass temperature $T_{\text{SG}}(B \rightarrow 0)$ (K)		130(5)	120(5)	110(20)	178(5)
freezing temperature $2a$ site at 7 T T_{OG} (K)		145(5)	135(5)		≈ 100
ordered moment $2a$ site at 4 K (μ_B)		0.89(6)	0.6(6)		≈ 2 8 at 7 T

^aAverage value.

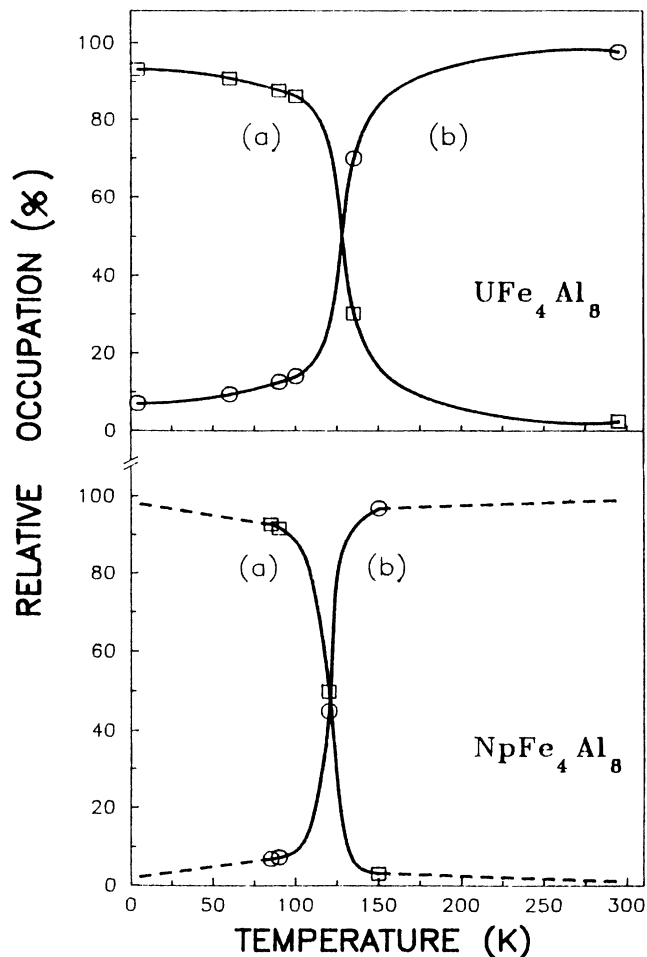


FIG. 6. Relative occupation of the (a) SG state and (b) paramagnetic state, which may serve as order parameters.

intensities, depending on the cooling history of the samples.

The NpFe_4Al_8 behaves similarly with one important difference: The enhancement of the (110) reflection starts only at ≈ 30 K with no indication of a transition in the region 30–300 K (Fig. 10).

For a perfectly ordered lattice, the enhancements of the (110), (310), (112), and (330) reflections are mainly due to an antiferromagnetic ordering of the $\text{Fe}(8f)$ sublattice, while the enhancements of the (200,101), (220,211), and (202,321) reflections arise mainly from the ferromagnetic

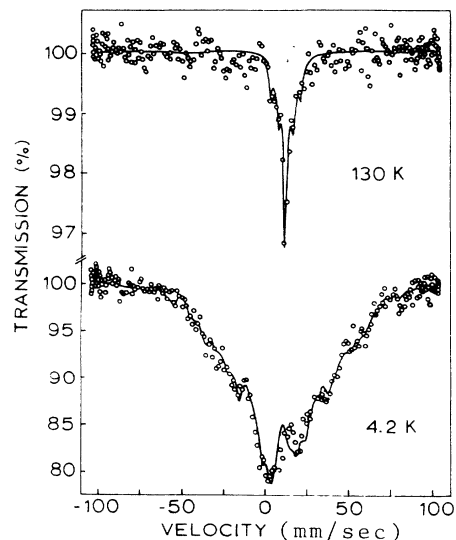


FIG. 7. ^{237}Np Mössbauer spectra of NpFe_4Al_8 at 4.2 and 130 K. The magnetic hyperfine fields decrease gradually with the temperature (see text).

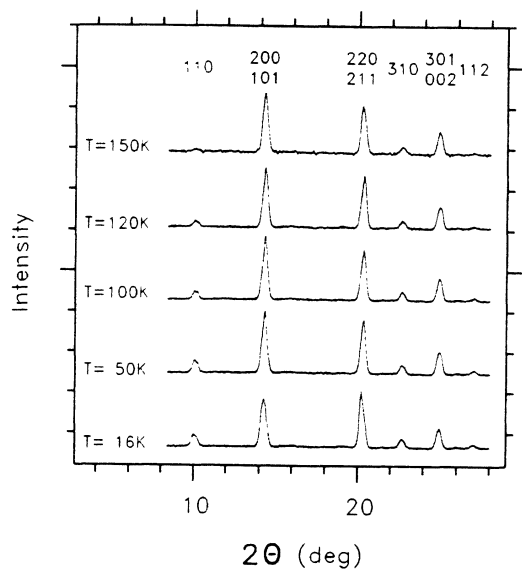


FIG. 8. Low-angle neutron-diffraction pattern of UFe_4Al_8 at the temperature range 16–150 K. Significant change of intensity is observed for the (110) reflection (see Fig. 9).

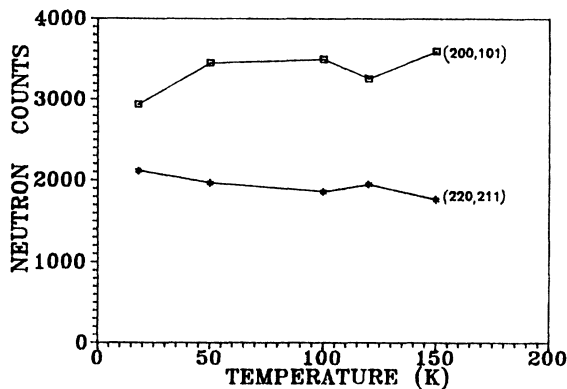
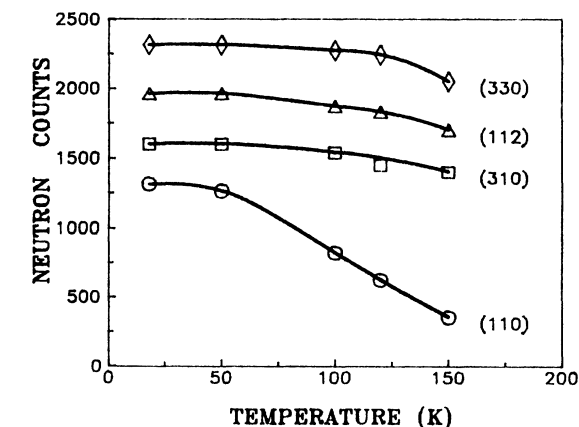


FIG. 9. Temperature dependence of integrated neutron-diffraction intensities of UFe_4Al_8 . The enhancements of the (110), (310), (112), and (330) reflections are due to an antiferromagnetic order of the Fe site, while the irregularities in the (200,101) and (220,211) reflections belong to the ferromagnetic U site.

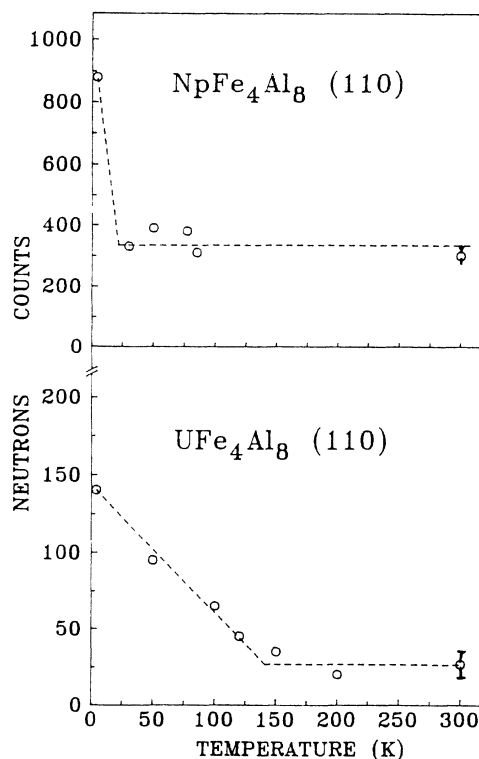


FIG. 10. Integrated intensity of the neutron reflection (110) of UFe_4Al_8 and NpFe_4Al_8 . Magnetic transitions occur below 150 and 30 K respectively.

ordering of the actinides at the $2a$ site.¹¹

The application of external magnetic fields from 2 to 7 T perpendicular to the neutron-scattering vector revealed enhancement of the (200,101) and (202,321) reflections, indicating ferromagnetic alignment of the A moments ($2a$ site) parallel to the magnetic field direction. This alignment is associated with strong preferred orientation effects of the grains in the powder even at room temperature. Patterns recorded at an applied field of 7 T are shown in Fig. 11. When switching off the applied field, the aligned moments remain frozen in the direction of the field for at least 48 h at 5 K. As shown in Fig. 11 at 7 T, the (110) and (220) reflections have disappeared due to orientation of the grains under the applied high field, establishing non-Bragg conditions for these reflections. We have calculated the intensities of the nuclear and magnetic reflections for oriented samples. As each of these reflections contains contributions from the Fe and A sites, it is impossible to calculate the saturated ordered moments per U and Np under applied magnetic fields. The temperature-dependent intensities of mainly the $2a$ sublattice reflections of the highly oriented UFe_4Al_8 sample are depicted in Fig. 12. From the (200,101) and (202,321,400) magnetic reflections, a transition is observed at ≈ 145 K, which coincides with the transition labeled T_{OG} mentioned above.

B. ThFe_4Al_8

The ac susceptibility of this compound is shown in Fig. 13. A transition with maximum at ≈ 110 K is clearly ob-

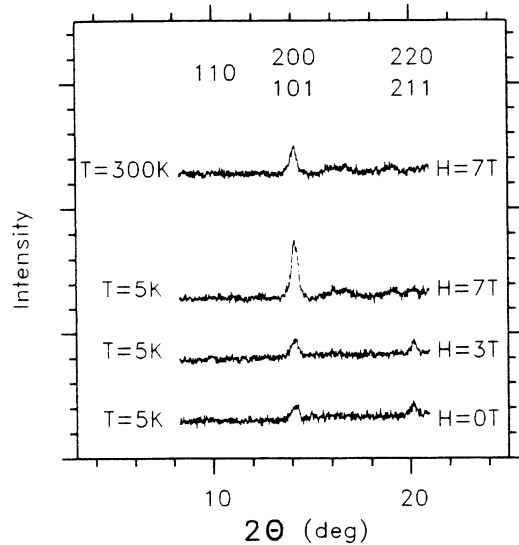


FIG. 11. Low-angle neutron-diffraction pattern of UFe_4Al_8 under applied magnetic field of 7 T perpendicular to the neutron beam. The disappearance of the (110) and (220,211) reflections is due to preferred orientation. Note that the powder grains remained highly oriented even after heating to room temperature. This figure should be compared to Fig. 8.

served. This transition is not of the sharp cusp type, and an upturn is already detectable at ≈ 130 K. The neutron-diffraction patterns show enhancements of the (110), (310), (112), and (330) reflections below 90 K. As an example, the integrated intensity of the (110) reflection is shown in Fig. 14. This has been previously interpreted as a result of antiferromagnetic ordering of the Fe(8f) sublattice.¹¹

The ^{57}Fe Mössbauer spectra reveal the onset of a magnetic hyperfine field splitting below ≈ 100 K, confirming the neutron-diffraction results, but somewhat lower than observed by the ac- and dc-susceptibility data.

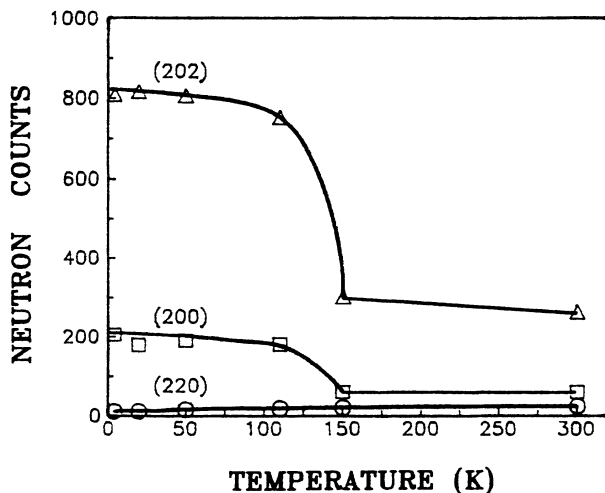


FIG. 12. Temperature dependence of integrated intensities of magnetic reflections of UFe_4Al_8 under an applied field of 7 T. This figure should be compared with Fig. 9.

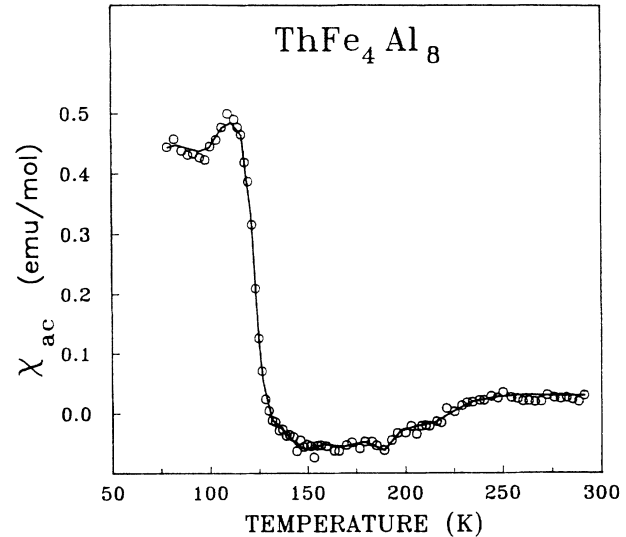


FIG. 13. ac susceptibility of ThFe_4Al_8 .

The dc magnetization measured in a field of 0.03 T shows a magnetic transition at ≈ 105 K. Thermoremanent magnetization effects at various applied fields are shown in Fig. 15. These effects point to a magnetic frustration in this compound. $T_{SG}(B)$, the SG temperatures at applied magnetic fields, are given in Fig. 4. $T_{SG}(0) \approx 100$ K is derived by extrapolation, in accord with the maximum observed in the ac susceptibility. The source of the frustration will be discussed below.

In summary, both UFe_4Al_8 and NpFe_4Al_8 show the following experimental results.

- A cusp in the ac susceptibility, the maximum of which we define as $T_{SG}(0)$ at 130 and 120 K, respectively.
- Irreversible components in the isothermal and thermoremanent dc magnetization below $T_{SG}(B)$ (T_{SG} is

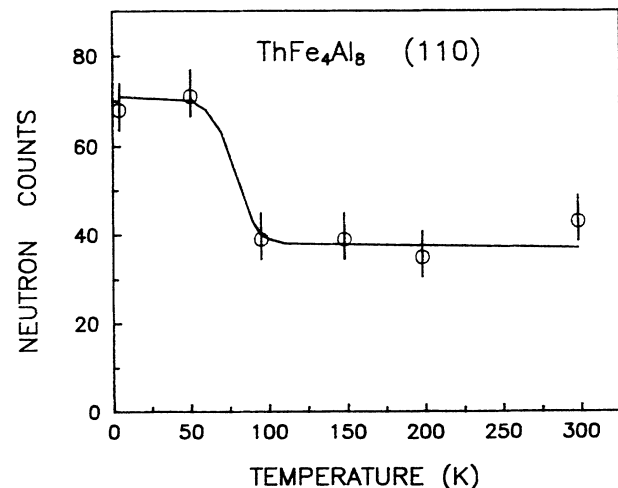


FIG. 14. Integrated intensity of the (110) reflection in ThFe_4Al_8 .

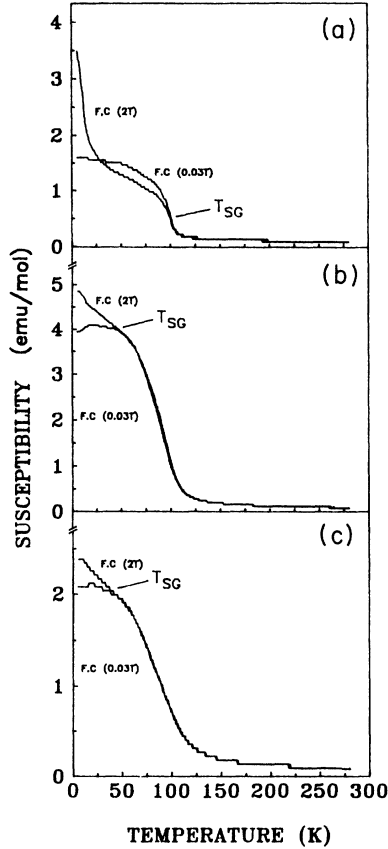


FIG. 15. Thermoremanent dc magnetization of ThFe_4Al_8 performed at various applied magnetic fields: (a) 0.03 T, (b) 0.1 T, and (c) 0.3 T. The sample was cooled under external magnetic fields of 0.03 and 2 T.

dependent on the applied magnetic field B).

(c) Onset of magnetic hyperfine fields at the ^{57}Fe nucleus ($8f$ site) and the ^{237}Np nucleus ($2a$ site) around $T_{\text{SG}}(0)$.

(d) High sensitivity to stoichiometry, cooling history, and annealing procedures.

(e) No indication of long-range magnetic order (magnetic Bragg scattering) at the A site in the vicinity of T_{SG} . However, we find indication of the non-Brillouin-like behavior deduced from the enhancement of the (110) magnetic reflection of the Fe sublattice below T_{SG} .

(f) The application of external magnetic fields causes alignment of the randomly oriented $5f$ moments parallel to the direction of the field. We show that

$$T_{\text{SG}}(7 \text{ T}) \rightarrow 0 \text{ and } T_{\text{SG}}(0 \text{ T}) \rightarrow T_{\text{OG}} \approx \text{const.}$$

As pointed out in the Introduction, all these findings can be related to the establishment of a spin-glass state,² and $T_{\text{SG}}(B)$ represents the SG transition temperature. Also, ThFe_4Al_8 should be assigned a spin-glass system with $T_{\text{SG}}(0) = 110(20)$ K, but its magnetic behavior is different as compared to the U and Np intermetallics (see Table I).

IV. DISCUSSION

During the past decade, unusual, irreversible magnetic phenomena have been reported on the body-centered tetragonal $R\text{Fe}_{4+x}\text{Al}_{8-x}$ ($R = \text{rare earth}$) (Ref. 6) and $A\text{Fe}_{4+x}\text{Al}_{8-x}$ systems.¹² Only recently were arguments put forward correlating these irreversibilities with the establishment of a spin-glass state in the R and Fe sublattices.^{5,13} Based on our experimental results, in the present discussion we argue that the UFe_4Al_8 , NpFe_4Al_8 , and ThFe_4Al_8 compounds should be assigned concentrated spin-glass systems.

An essential proof for a SG state comes from the ^{237}Np and ^{57}Fe Mössbauer spectra which reveal magnetic splittings, indicating local spin ordering below $T_{\text{SG}}(0)$. The reduction in the quadrupole interaction by a factor of ≈ 2 between the paramagnetic and magnetic states derived from the ^{57}Fe spectra is an indication that the direction of the Fe moments and electric field gradient are perpendicular. This is usually taken as an argument for a conventional magnetic ordering and against the SG picture. We put forward another possible explanation, namely, that the Fe spins are randomly frozen within the tetragonal basal plane perpendicular to the tetragonal c direction,¹⁴ where frustration in the $8f$ sublattice comes from the conflict between the ferromagnetic and antiferromagnetic components of the Fe moments, leading to asymmetric (odd) basal plane configurations in the $I4/mmm$ tetragonal structure (G type).¹¹ Such a frustration is described basically by the Anderson model for a $d=2$ SG system.¹⁵ This would explain the frustration observed experimentally in both ThFe_4Al_8 (Refs. 12 and 16) and YFe_4Al_8 ,¹³ where no conflicting interaction between the $2a$ and $8f$ sites occurs.

The broad distribution of the hyperfine fields in the temperature region between 4.2 and 120 K as observed at the ^{237}Np nucleus (Fig. 7) is in accord with the establishment of a SG state.

When decreasing the temperature, the data of UFe_4Al_8 given in Figs. 9 and 10 show a linear enhancement of the (110), (310), (112), and (330) reflections. This points to a gradual spin freezing of the Fe sublattice below 140 K. It could be correlated to the frustration of antiferromagnetic iron moments at the $8f$ site in the tetragonal symmetry, similar to ThFe_4Al_8 and YFe_4Al_8 intermetallics, and could hint to a hierarchical configurational ordering,¹⁷ where an antiferromagnetic state should be reached at lowest temperatures. In fact, previous analysis of the present neutron-diffraction data revealed that, below 16 K, the Fe($8f$) sublattices of the $A\text{Fe}_4\text{Al}_8$ ($A = \text{Th, U, Np}$) intermetallics are antiferromagnetically ordered, independently of the actinide partner.¹⁸ However, the neutron data indicate the presence of a nonsaturated magnetic order at the U and Np sublattices even at 4.2 K. For this reason the magnetic character of the A site was further tested by neutron diffraction under external magnetic fields; after switching off the field, at 4.2 K, the U and Np moments stayed ferromagnetically aligned, frozen parallel to applied field for longer than 48 h. This was deduced from the enhancement of the (200,101) and (202,321,400) magnetic reflections (Fig. 12). It means

that spin freezing conditions exist also in the A site, and the question is whether the freezing temperature of the actinide moments under field coincides with T_{SG} . The comparison of the neutron-diffraction experiments with and without applied magnetic field (as shown, e.g., for U) in Figs. 9 and 12 confirms the establishment of an aligned spin state at the U and Np sublattices below ≈ 145 and 130 K, respectively, in agreement with the magnetic transitions observed by our ac- and dc-susceptibility and Mössbauer data. We label the ordering temperature of aligned A spins, frozen ferromagnetically, T_{OG} . As shown, $T_{\text{OG}} \geq T_{\text{SG}}(B)$ and serves as the upper limit of the freezing temperature (ferromagnetic and antiferromagnetic), of both the $2a$ and $8f$ sites.

A decrease of T_{SG} with increase of B is predicted by several theoretical models for Fe($3d$) spin glasses.^{19,20} The majority of the experimental results are in favor of the de Almeida–Thouless (AT) approach, indicating a nonlinear behavior of $\tau_c = 1 - T_{\text{SG}}(B)/T_{\text{SG}}(0) \propto B^\theta$.²⁰ As the itinerant character of the $5f$ and $3d$ electrons in a metal are similar, we expect the AT line to hold also for the U and Np spin glasses. As shown in Fig. 16, an AT line taking $\theta = \frac{2}{3}$ fairly fits the experimental data.

Interesting is the decrease of T_{SG} with an increase of B and the relation $T_{\text{SG}}(B \rightarrow 0) \leq T_{\text{OG}}$. This behavior is totally different as compared to HoFe_4Al_8 , where T_{OG} represents a transition from an aligned to a random SG state, and increases with the increase of the applied field B . In addition, $T_{\text{SG}} \gg T_{\text{OG}}(B)$.⁵ For the present A SG systems under a strong applied magnetic field, T_{OG} is nearly a constant and serves as the ordering temperature of a phase transition. These differences may be explained on the basis of the large spatial distribution of the $5f$ -electron wave functions, revealing a long-range character of the interactions in a $5f$ SG system. Mediated by the Al $3p$ electrons, f - p and f - d electron hybridization leads to practically the same freezing temperatures of the A ($2a$) and Fe($8f$) sites. The localized character of the $4f$ -electron moment seems to be the reason for the unusual behavior of T_{OG} in HoFe_4Al_8 , as seen, e.g., in the field dependencies of T_{OG} and T_{SG} .

Our data provide sufficient arguments for declaring UFe_4Al_8 and NpFe_4Al_8 spin-glass systems for which the relative occupation of the paramagnetic state, as derived from the Mössbauer ^{57}Fe spectra (Fig. 6), may serve as the ordering parameter q .¹

It remains to explain the source of the randomness of the spin orientation and the reason for the conflicting interactions: At low temperatures the U and Np sublattices in the $A\text{Fe}_4\text{Al}_8$ systems tend to order ferromagnetically, while the Fe sublattice orders antiferromagnetically.¹¹ As shown above, there exists *a priori* frustration within the antiferromagnetic spin configuration of the Fe as observed for YFe_4Al_8 and ThFe_4Al_8 . But the main frustration in the present system is due to the conflicting Ruderman–Kittel–Kasuya–Yosida interaction between the Fe and A moments (compare, for example, Figs. 3 and 15). The random distribution of Al vacancies together with Fe ($\approx 4\%$) atoms at the $8j$ site is also a source for randomness in the system.^{5,10} In total, this leads to the

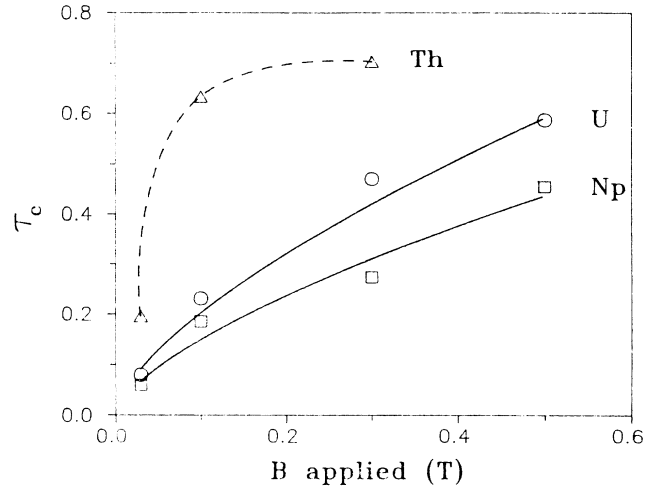


FIG. 16. $\tau_c = 1 - T_{\text{SG}}(B)/T_{\text{SG}}(0)$ vs the applied field B . The solid line represents the de Almeida–Thouless line with $\theta = \frac{2}{3}$ (Ref. 20) (see text). The dashed line is a guide to the eye. (Δ) ThFe_4Al_8 , (\circ) UFe_4Al_8 , and (\square) NpFe_4Al_8 .

establishment of a SG state in both $R\text{Fe}_4\text{Al}_8$ and $A\text{Fe}_4\text{Al}_8$ ($A = \text{U}, \text{Np}$) compounds. The sharp cusps observed in χ_{ac} in the present compounds is thus in accord with the SG picture. For comparison we show the ac susceptibility of the isostructural HoFe_4Al_8 , which in a previous publication was shown also to be a SG.⁵ The absence of a cusp or, at most, an extremely broad maximum is observed (Fig. 1). Therefore, in general, the presence of a cusp in the ac susceptibility for a frozen spin system, dilute or concentrated, is not necessarily indicative of a SG transition, and it is an insufficient criterion for declaring a SG state. Snapshots with different time windows (Mössbauer, ac- and dc-susceptibility, and neutron-diffraction methods) must be used to confirm the presence of a SG state.

V. CONCLUSIONS

We have shown that the spin-glass temperature $T_{\text{SG}}(B)$ is a reproducible parameter independent of the observation time window. This argues for a true thermodynamic phase transition at T_{SG} . Unfortunately, specific-heat measurements are not available for the present systems. Such measurements, in particular after switching off an applied magnetic field, would help to clarify this point.

ACKNOWLEDGMENTS

One of us (J.G.) would like to thank I. Nowik and I. Felner for many illuminating discussions. This work was funded by the German Federal Minister for Research and Technology (BMFT) under Contract Nos. 03-GA2BEE, 03-KA2TUM, 03-WI2BON, and by the National Council for Research and Development, Israel.

- ¹D. Staufer and K. Binder, *Z. Phys. B* **30**, 313 (1978).
- ²D. Chowdhury, *Spin Glass and Other Frustrated Systems* (World Scientific, Singapore, 1986), p. 1 and 31.
- ³I. Yeung, W. Ruan, and R. M. Roshko, *J. Magn. Magn. Mater.* **74**, 59 (1988).
- ⁴D. C. Rapaport, *J. Phys. C* **10**, L543 (1978).
- ⁵J. Gal, I. Yaar, E. Arbaboff, H. Etedgi, F. J. Litterst, K. Aggarwal, J. A. Pereda, G. M. Kalvius, G. Will, and W. Schafer, *Phy. Rev. B* **40**, 745 (1989).
- ⁶I. Felner and I. Nowik, *J. Phys. Chem. Solids* **39**, 951 (1978).
- ⁷W. Schäfer, E. Jansen, F. Elf, and G. Will, *J. Appl. Crystallogr.* **17**, 159 (1984).
- ⁸S. Tapuchi, Ph.D thesis, Ben-Gurion University, Beer Sheva, Israel, 1988.
- ⁹E. Arbaboff, MSc. thesis, Ben-Gurion University of the Negev, Beer Sheva, Israel, 1989.
- ¹⁰J. Gal, H. Pinto, S. Fredo, H. Shaked, W. Schäfer, G. Will, F. J. Litterst, W. Potzel, L. Asch, and G. M. Kalvius, *Hyperfine Interact.* **33**, 173 (1987).
- ¹¹W. Schafer, M. Gronefeld, G. Will, and J. Gal, *Mater. Sci. Forum* **27-28**, 243 (1988); and (unpublished).
- ¹²A. Baran, W. Suski, and T. Mydlarz, *Physica* **130B**, 219 (1985).
- ¹³F. Felner and I. Nowik, *J. Magn. Magn. Mater.* **74**, 31 (1988).
- ¹⁴M. Grönefeld, diploma thesis, Mineralogisches Institut, Bonn University, West Germany, 1987.
- ¹⁵P. W. Anderson, *J. Less-Common Met.* **62**, 291 (1978).
- ¹⁶I. Felner and I. Nowik, *J. Magn. Magn. Mater.* **58**, 169 (1986).
- ¹⁷S. R. McKay, A. N. Berker, and S. Kirkpatrick, *J. Appl. Phys.* **53**, 7974 (1982).
- ¹⁸W. Schäfer, G. Will, J. Gal, and W. Suski, *J. Less-Common Met.* **149**, 237 (1989).
- ¹⁹S. M. Dubiel, K. H. Fischer, Ch. Sauer, and W. Zinn, *Phys. Rev. B* **36**, 360 (1987).
- ²⁰R. L. de Almeida and D. J. Thouless, *J. Phys A* **11**, 983 (1978).